Journal of Power Sources 261 (2014) 249–254

Contents lists available at ScienceDirect

Journal of Power Sources

journal homepage: www.elsevier.com/locate/jpowsour

Short communication

Synthesis and characterization of multi-layer core–shell structural $LiFeBO_3$/C as a novel Li-battery cathode material

Bao Zhang, Lei Ming, Jun-chao Zheng*, Jia-feng Zhang, Chao Shen, Ya-dong Han, Jian-long Wang, Shan-e Qin

School of Metallurgy and Environment, Central South University, Changsha 410083, PR China

HIGHLIGHTS

- $LiFeBO_3$/C was prepared by spray-drying and carbothermal method for the first time.
- The novel structure improved the conductivity and prevented it from air erosion.
- It presents better electrochemical performance than previously reported.

ARTICLE INFO

Article history:
Received 9 December 2013
Received in revised form
26 January 2014
Accepted 19 March 2014
Available online 28 March 2014

Keywords:
Lithium iron borate
Spray-drying
Cathode material
Electrochemical properties

ABSTRACT

A multi-layer core–shell structural $LiFeBO_3$/C has been successfully synthesized via spray-drying and carbothermal method using $LiBO_2 \cdot 8H_2O$, $Fe(NO_3)_3 \cdot 9H_2O$, and citric acid as starting materials. The Rietveld refinement results indicate the sample consists of two phases: $LiFeBO_3$ [94(6)% w/w], and $LiFeO_2$ [6(4)% w/w]. SEM images show that the $LiFeBO_3$ powders consist of rough similar-spherical particles with a size distribution ranging from 1 μm to 5 μm. TEM results present that the $LiFeBO_3$ spherical particles are well coated by nano-carbon webs and form a multi-layer core–shell structure. The amount of carbon was determined to be 6.50% by C/S analysis. The prepared $LiFeBO_3$–$LiFeO_2$/C presents an initial discharge capacity of 196.5 mAh g^{-1} at the current density of 10 mA g^{-1} between 1.5 and 4.5 V, and it can deliver a discharge capacity of 136.1 mAh g^{-1} after 30 cycles, presents excellent electrochemical properties, indicating the surface sensitivity in the air was restrained.

1. Introduction

Lithium ion batteries, due to their large gravimetric, volumetric energy densities and other advantages including low price, long cycle-life and environmental friendly, are currently considered the most advanced electrical energy storage and transfer system [1]. At present, most of the lithium batteries used in electronic devices or hybrid electric vehicles employ transition metal oxides such as $LiCoO_2$, $LiMn_2O_4$ or mixed metal analogs such as $Li(Ni, Mn, Co)O_2$ as the active cathode materials [1,2]. But their high cost, toxicity, and other disadvantages prohibit their large-scale application for lithium ion batteries, such as plug-in hybrid vehicles. $LiFePO_4$ was considered as one of the promising candidates since it was first reported in 1997 [3–5], because of its low cost and plentiful elements and environmentally benign. However, its low energy density and low conductivity have driven researchers to find other substitutes.

Metal-borate materials have been regarded as the promising cathode alternative for lithium ion batteries due to its higher theoretical capacity (~220 mAh g^{-1}), small volume change (ca. 2%) [6–8], and its favorable chemical constituents, which are abundant, inexpensive and non-toxic. And it is well known that boron atom can be coordinated by oxygen atoms to form a variety of atomic groups, which are considered to be a dominant factor for physical properties. In addition, it has been shown that polyanions enable low transition metal redox energies through the inductive effective effect, thereby allowing some sort tuning of such energies. From the thermo-dynamic study performed in the case of $LiFeBO_3$, the Fe^{3+}/Fe^{2+} reduction couple lies between 3.1 V/Li and 2.9 V/Li, demonstrating an important inductive effect of the BO_3 group. It should be a good cathode material for lithium-ion batteries. The electrochemical performance of $LiFeBO_3$ was first

* Corresponding author. Tel.: +86 731 88836357.
E-mail addresses: jczheng@csu.edu.cn, tonyson_011@163.com (J.-c. Zheng).

http://dx.doi.org/10.1016/j.jpowsour.2014.03.082
0378-7753/

investigated in 2001 with a reported capacity of less than 10 mAh g^{-1} under an extremely low rate (C/250) [6]. Recently, Yamada and coworkers achieved a large reversible capacity of approximately 190 mAh g^{-1} by carefully preparing electrode sample under an inert Ar atmosphere [8]. They attributed the performance improvement to the prevention of air exposure. If the $LiFeBO_3$ is wrapped by nano-carbon webs, and form a multi-layer core–shell structure (as the schematic illustration shown in Fig. 1), it may improve the conductivity of the $LiFeBO_3$ and also prevent it from the air corrosion.

Spray-drying is an effective method to mix raw materials by solution process at a molecular size level and to easily obtain spherical particles. It is a method well-known for synthesizing multi-component and fine homogeneous powder samples [9–12]. Nevertheless, $LiFeBO_3$ synthesized via spray-drying process has not been studied or reported yet. In this work, we try to prepare a multi-layer core–shell $LiFeBO_3$/C via spray-drying process followed by carbothermal method, the structures and electrochemical performances of the synthesized samples are studied.

2. Experimental

First, the stoichiometric amount of $LiBO_2{\cdot}8H_2O$ (AR, 99%), $Fe(NO_3)_3{\cdot}9H_2O$ (AR, 98.5%), and citric acid (AR, 99.5%) were dispersed in the deionized water. The mixture was stirred at 80 °C until the homogeneous bright yellow sol was obtained. Second, the sol was dried to form the precursor via a spray-dryer, the air pressure is 0.25 MPa, the inlet and outlet air temperatures were 230 °C and 120 °C, respectively. Then, the as-prepared precursor were transferred into a tube furnace and heated to 300 °C at a heating rate of 2 °C min^{-1} for 2 h under the Ar atmosphere to decompose nitrates and carbohydrate reagent, followed by cooling down to room temperature naturally. At last the samples were carefully grinded by mortar, then sintered at 550 °C for 10 h to yield $LiFeBO_3$/C composite. The synthesis process for the $LiFeBO_3$/C composites is schematically illustrated in Fig. 1.

The surface element's content of powders was determined by X-ray photoelectron spectrometer (XPS, Kratos Model XSAM800) equipped with Mg Kα achromatic X-ray source (1235.6 eV). Structural and crystalline phase analysis of the products was taken from the powder X-ray diffraction (XRD, Rint-2000, Rigaku) using CuKα radiation. Elemental carbon analysis of sample was performed by C–S analysis equipment (Eltar, Germany). The samples were observed by SEM (JEOL, JSM-5600LV) and a Tecnai G12 transmission electron microscope (TEM).

The electrochemical characterizations were performed using CR2025 coin-type cell. Typical positive electrode loadings were in the range of 2–2.5 mg cm^{-2}, and an electrode diameter of 14 mm was used. The cathode of the two-electrode electrochemical cells was fabricated by blending the powders with super P and polyvinylidene fluoride (PVDF) binder in a weight ratio of 8:1:1 in N-methyl-2-pyrrolidone (NMP). Then the mixed slurry was coated uniformly on aluminum foil, dried in the oven for 4 h at 120 °C. The assembly of the cells was carried out in a Mikrouna glove box filled with high-purity argon where the lithium metal foil was used as an anode, Celgard2320 as separator. The electrochemical measurements were performed using a LAND CT2001A battery tester (LAND, China) in the voltage range between 1.5 and 4.5 V at room temperature (25 °C). The cyclic voltammetry measurements were carried out at the scan rate of 0.1 mv s^{-1} in the voltage range of 1.5–4.5 V with a CHI660D electrochemical analyzer.

3. Results and discussion

The structure of the synthesized sample was determined by using the powder X-ray diffraction, the results are shown in Fig. 2. The diffraction peaks of sample can be regarded as monoclinic $LiFeBO_3$ with space group of $C2/c$. The observed XRD reflections highly resemble the previously reported patterns [6–8]. In order to clarify the structure of $LiFeBO_3$ sample, XRD data are refined by Rietveld method. The refinement results and crystal parameters of are shown in Fig. 2(a) and Table 1, respectively. As shown, the observed and calculated patterns match well, and the reliability factors are good. According to the refinement results, $LiFeBO_3$ has lattice parameters a = 5.1728(1) Å, b = 8.9240(1) Å, c = 10.1475(3) Å, β = 91.1208°. The results compared well with those reported by Atsuo Yamada [8] (a = 5.1597(2) Å, b = 8.9127(5) Å, c = 10.1559(4) Å, β = 91.34(3)°) and Y. M. Zhao [14] (a = 5.166(2) Å, b = 8.919(2) Å, c = 10.1135(3) Å, β = 91.39(2)°). Most of the Bragg peaks agree well in position and relative intensity with those reported by Atsuo Yamada [8,13]. The refinement results (Table 1) show that the atoms positions and occupancy for Li and Fe atoms and the ball & stick representation of 3D structure of $LiFeBO_3$ along [111] are in good agreement with the earlier work [6]. The Rietveld refinement results indicate the sample consists of two phases: $LiFeBO_3$ [94(6)% w/w], and $LiFeO_2$ [6(4)% w/w]. A similar kind of impurity ($LiFeO_2$) was noticed by Y. M. Zhao et al. [14]. Carbon remaining in the composite was not detected, which indicates the residual carbon is amorphous. The amount of carbon in the composite is about 6.5wt.% determined by C–S analysis method.

Further details on the structure of the synthesized $LiFeBO_3$ samples were acquired via X-ray photoelectron spectroscopy (XPS) analysis. Fig. 3 shows the XPS spectra of the $LiFeBO_3$ samples. It is clear that the signals of Li, Fe and O are present in the spectrum, and C1s is also detected at 284.5 eV, which is assigned to the pyrolytic carbon. The binding energy (BE) values of Fe2p are 711.28 eV and 725.18(±0.2) eV, which correspond to energy level Fe2p3/2 and Fe2p1/2, respectively. According to the reference [15], Fe^{3+} (Fe_2O_3) cation exhibits characteristic peak of Fe2p3/2 at 709.7 eV, Fe^{2+} (FeC_2O_4) cation exhibits peak of $Fe2p_{3/2}$ at 712.1 eV. It can be seen

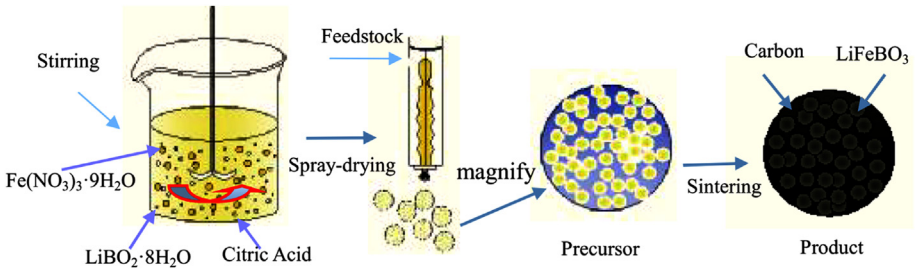

Fig. 1. Schematic illustration of fabrication process for $LiFeBO_3$/C.

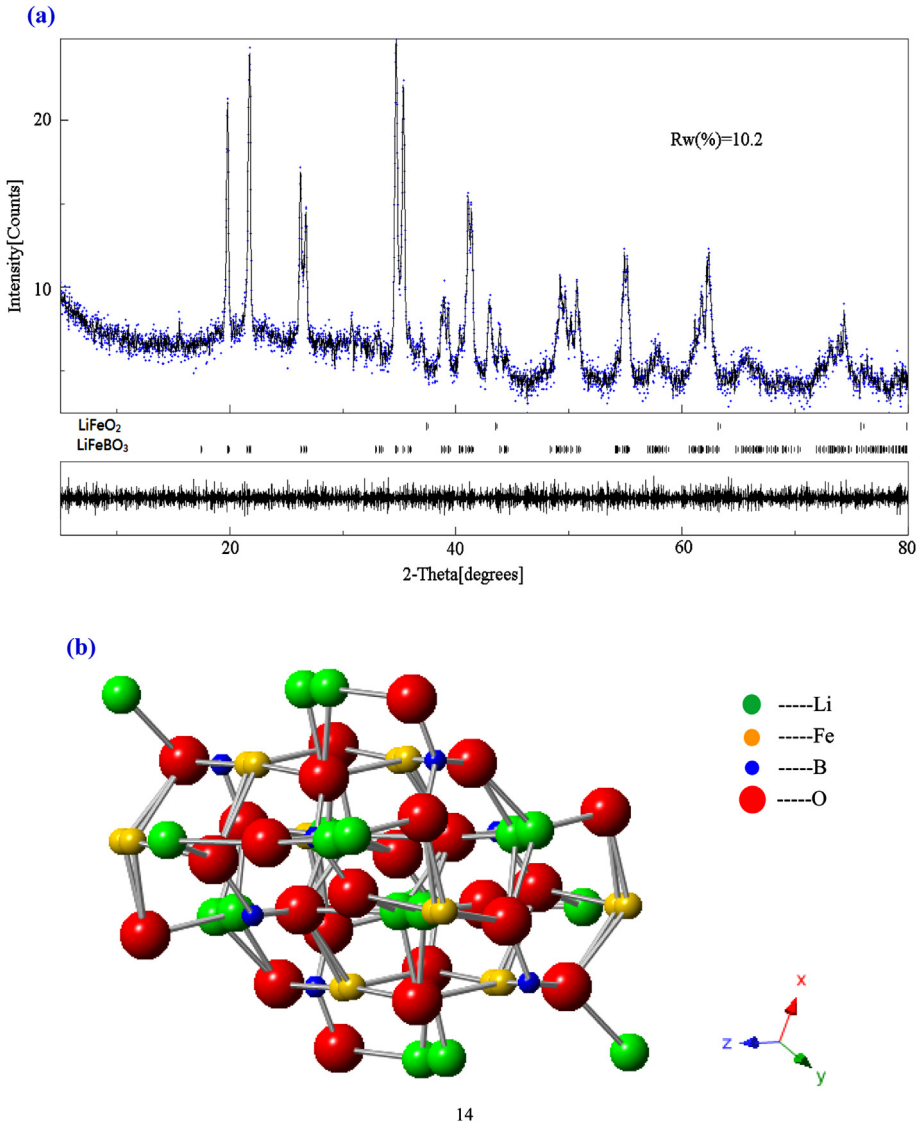

Fig. 2. (a) Rietveld refinement of the $LiFeBO_3$/C XRD data; (b) Ball & stick representation of 3D structure of $LiFeBO_3$ along [111].

that the sample present a peak at binding energy (711.28 eV) comparable to the one observed in FeC_2O_4 (712.1 eV), and is much higher than the one of the Fe_2O_3 (709.7 eV). The results reveal that the valence states of Fe in the sample are +2 and +3. The O1s spectrum has a BE value of 531.88 eV, shown in Fig. 3, similar to the BEs reported for O1s in $LiFePO_4$ (531.6 and 533.2 eV) [16]. It is concluded that the XPS data indeed show the expected valence states of the metal and non-metal ions in $LiFeBO_3$ and $LiFeO_2$. The results are in accordance with XRD data.

Table 1
Results of structural analysis obtained from X-ray Rietveld refinement of $LiFeBO_3$.

Atom	Site	*x*	*y*	*z*	Occupancy
Li1	8f	0.6099(8)	0.5054(1)	0.1269(9)	0.48
Li2	8f	0.6912(0)	0.4732(7)	0.0013(2)	0.52
Fe1	8f	0.1627(4)	0.3307(0)	0.1375(8)	0.72
Fe2	8f	0.1801(3)	0.3443(6)	0.1036(8)	0.28
B1	8f	0.1180(0)	0.6783(4)	0.1347(3)	1
O1	8f	0.4338(7)	0.1615(5)	0.0798(6)	1
O2	8f	0.8018(5)	0.3338(5)	0.1540(2)	1
O3	8f	0.2991(4)	0. 5386(6)	0.1275(4)	1

Space group: $C2/c$:$b1$. $R_{wp} = 10.2\%$.
Cell constant: $a = 5.1728(1)$ Å, $b = 8.9240(1)$ Å, $c = 10.1475(3)$ Å, $\beta = 91.1208°$.

Fig. 4 shows the SEM and TEM images of the as-prepared $LiFeBO_3$/C samples, Fig. 4(a) and (b) presents a rough similar-spherical particles with a size distribution ranging from 1 μm to 5 μm, the $LiFeBO_3$/C particles show good uniformity and have no coalescence. As shown in Fig. 4(b), the spherical particles are actually an aggregation of some smaller particles of several hundred nanometers linked by the pyrolytic carbon. To further investigate the nature of surface coating and carbon distribution in the powders, we did TEM analysis, as shown in Fig. 4(c) and (d). The Fig. 4(c) shows the prime $LiFeBO_3$/C particles are well wrapped with a nano-scale carbon layer (internal surface area of the sample). The Fig. 4(d) shows that the thickness of the carbon coating in the external surface area of the samples has been calculated to be about 2 nm. The spherical $LiFeBO_3$/C particles are linked by nano-sized web of amorphous carbon, and form a multi-layer core–shell structure, the morphology is schematically illustrated in Fig. 1. This multi-layer core–shell structure is very useful for improving the conductivity of the samples, and preventing it from air corrosion when $LiFeBO_3$ exposed in the air. So

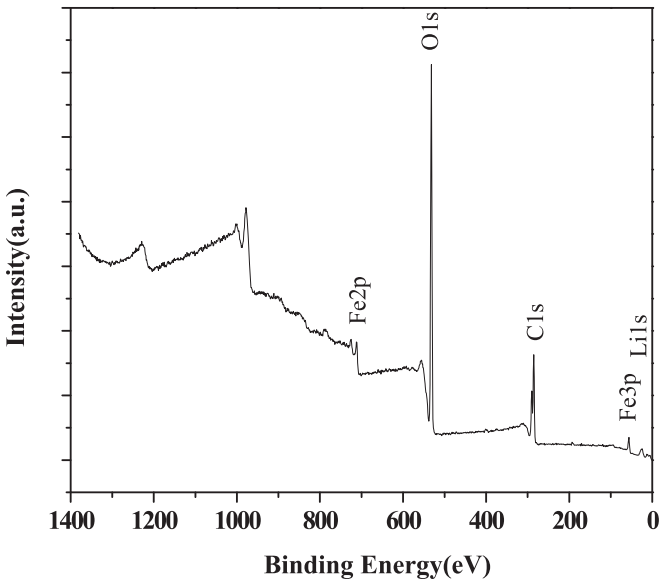

Fig. 3. XPS spectra of $LiFeBO_3$/C powders.

this multi-layer core–shell $LiFeBO_3$/C tends to deliver excellent electrochemical performance.

Fig. 5 shows the charge and discharge curves of the Li/$LiFeBO_3$–C cell cycled in the voltage range between 1.5–4.5 V at ambient temperature conditions. The voltage profiles exhibit two charge plateaus and the corresponding two discharge ones, which correspond to the plateaus of $LiFeBO_3$ (2.8–3.2 V) and $LiFeO_2$ (2.1–2.6 V). The results are in accordance with XRD and XPS data. As shown in Fig. 5, an initial discharge capacity about 196.5 mAh g^{-1} was obtained at the discharge current density of 10 mA g^{-1}, reaching 87.8% of the theoretical capacity of $LiFeBO_3$–$LiFeO_2$ (The theoretic specific capacity (C_T) of $LiFeBO_3$–$LiFeO_2$ is calculated with the following equation: $C_T = (220X_1 + 282X_2)$ (mAh g^{-1}), where 220 and 282 are the theoretic capacities of $LiFeBO_3$ and $LiFeO_2$ (<4.5 V), respectively; X_1 and X_2 are the weight content of $LiFeBO_3$ and $LiFeO_2$, respectively. Based on our Rietveld refinement results, the weight ratio of $LiFeO_2$ is 6%, so the C_T for $LiFeBO_3$–$LiFeO_2$ synthesized in this paper is 223.7 mAh g^{-1}). And the real capacity of the synthesized $LiFeBO_3$ is about 186 mAh g^{-1}, and about 10 mAh g^{-1} for the $LiFeO_2$.

Fig. 5(b) and Fig. 6 demonstrate the rate and cycle performance of the $LiFeBO_3$/C composite material in the voltage range 1.5–4.5 V in the Li/$LiFeBO_3$ cell. The current rate was changed from 10 mA g^{-1} to 20 mA g^{-1}, then 40 mA g^{-1} and at last returned to 10 mA g^{-1} in sequence for 30, 20, 10, and 20 cycles respectively. The initial discharge capacities are 196.5 mAh g^{-1}, 135.6 mAh g^{-1}, 96.2 mAh g^{-1} and 126.0 mAh g^{-1}, respectively, which is much better than previously reported [6,14,19]. When the current density is increased to 40 mA g^{-1} at 50th, the specific capacity decreased to 96.2 mAh g^{-1}, whereas when the current density is decreased to 10 mA g^{-1} again, the discharge capacity return to 126.0 mAh g^{-1} at 60th, which illustrating that the structure of the multi-layer core–shell $LiFeBO_3$/C keeps stable after cycling.

Besides, the charge curve in the first cycle is completely different from the following cycles, the specific capacity is much lower and the voltage plateau is higher, it is mainly caused by the $LiFeO_2$ phase [17,18]. The results are the same as Zhao et al. reported [14].

What's more important, during our experiment the whole process, except for the sintering and coin cell fabrication procedures, were all operated in the air. Considering the fact that the

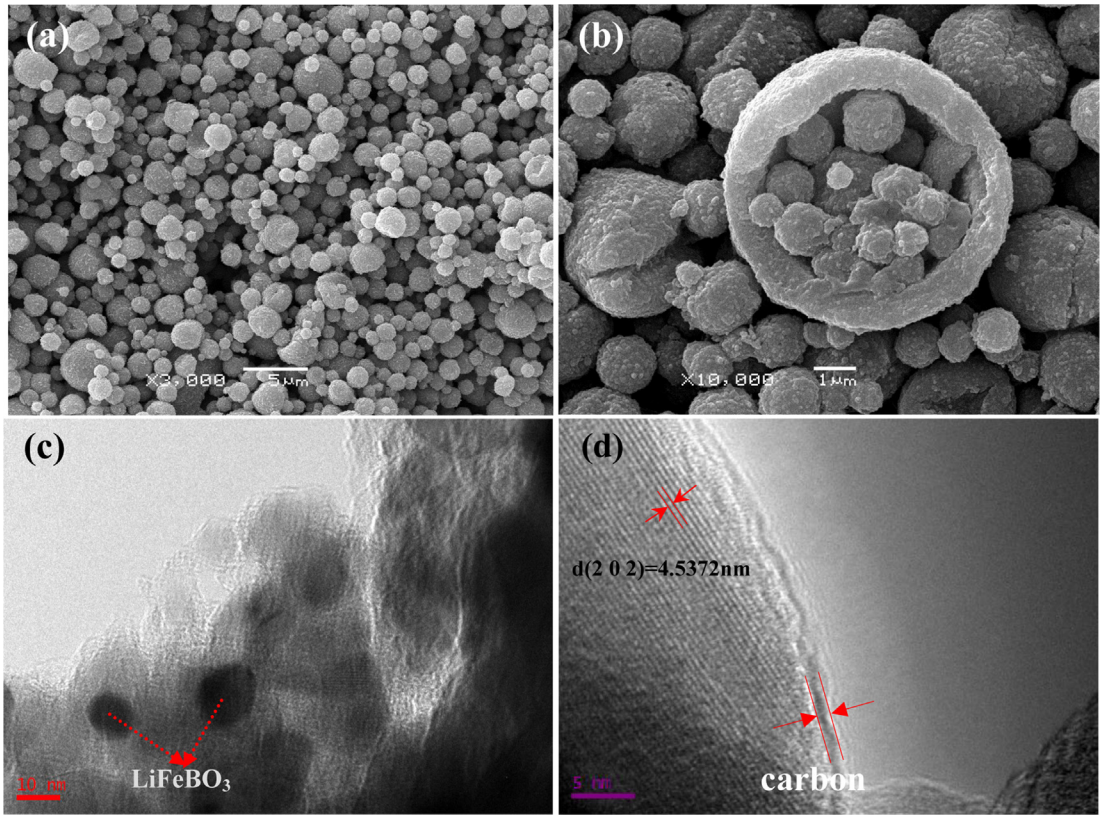

Fig. 4. (a) Low-magnification and (b) high-magnification SEM images of $LiFeBO_3$/C, (c) (d) TEM images of $LiFeBO_3$/C.

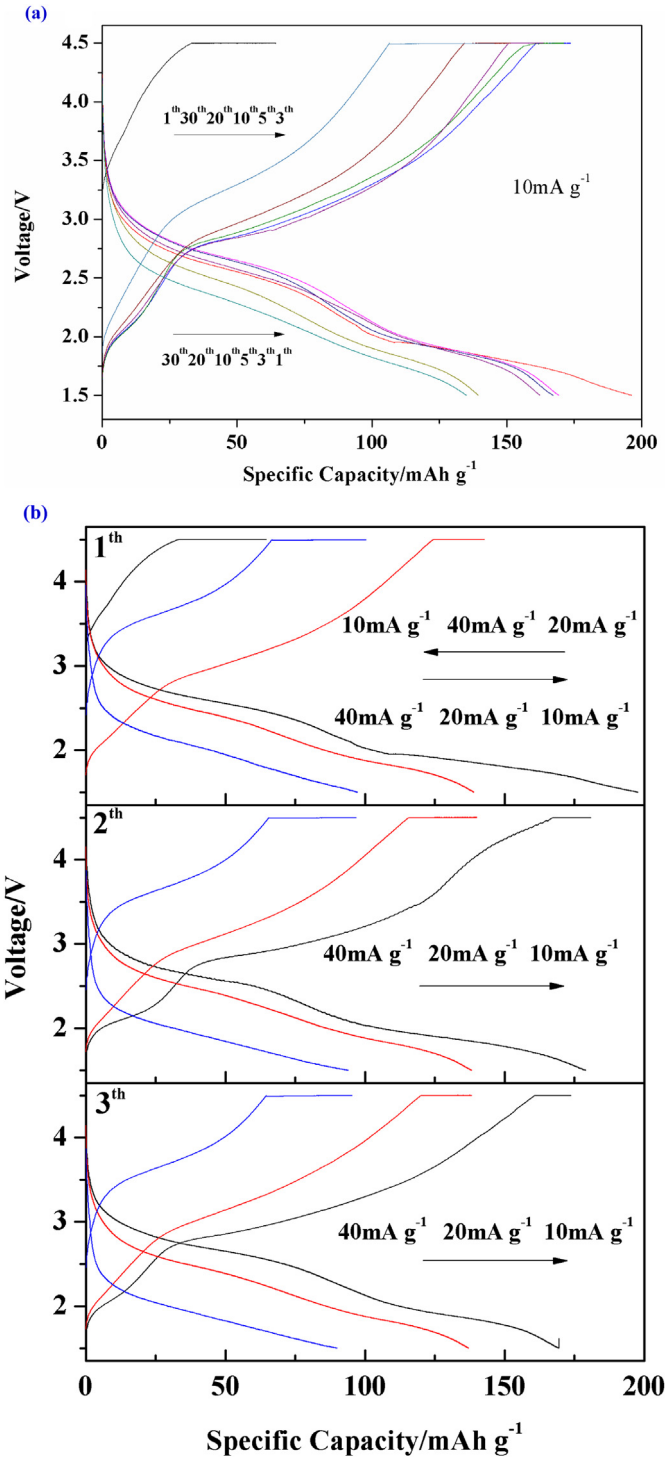

Fig. 5. (a) Charge and discharge curves of the $LiFeBO_3$/C during different cycles at 10 mA g^{-1}. (b) Charge and discharge curves of the $LiFeBO_3$/C during the first three cycles at different rates.

surface of $LiFeBO_3$ material is very sensitive to the air, when contact with moisture in the air, it tends to induce severe degradation of electrode properties [8,13,19]. However, in our experiment, the electrochemical performance of synthesized $LiFeBO_3$/C is excellent as depicted in Fig. 5. Therefore, We have reason to believe that "surface poisoning" of $LiFeBO_3$ is effectively restrained because of the multi-layer core–shell structure.

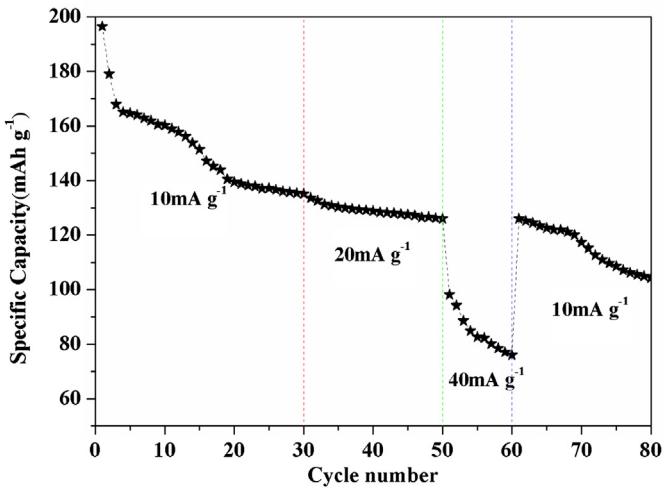

Fig. 6. Discharge capacities vs. cycles of $LiFeBO_3$ at different current density in the voltage range: 1.5–4.5 V.

The CV curve was recorded in the potential range of 1.5–4.5 V for the $LiFeBO_3$/C system is shown in Fig. 7. It shows that the oxidation and reduction peaks appear in the way of the superimposition of the peaks of $LiFeBO_3$ and $LiFeO_2$. No other peaks can be

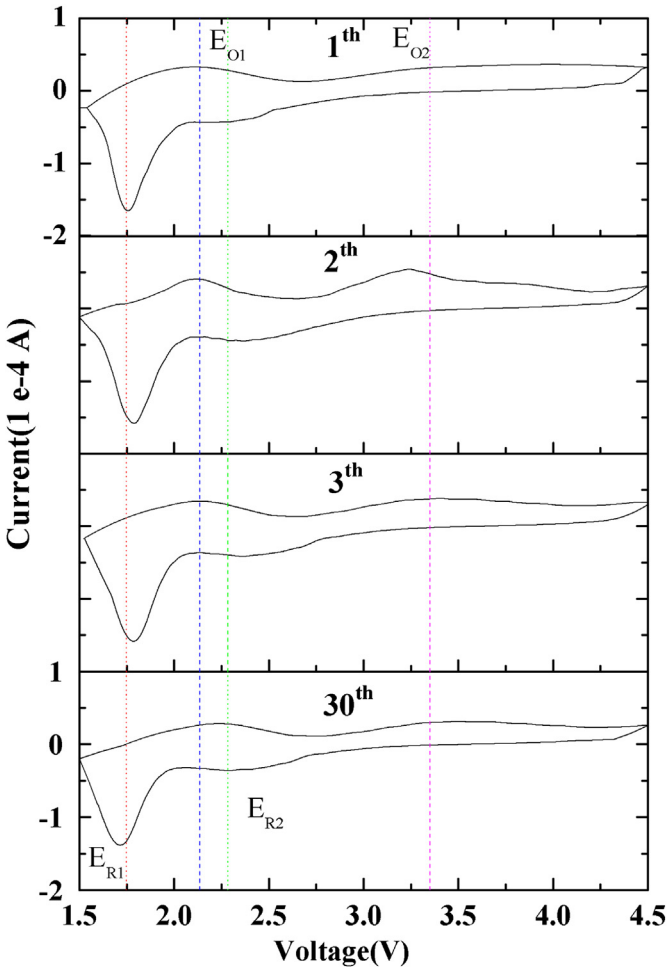

Fig. 7. Cyclic voltammograms of $LiFeBO_3$/C at a scan rate of 0.1 mv s^{-1} in the potential range of 1.5–4.5 V.

Table 2
Potentials of anodic and cathodic peaks shown in Fig. 7.

Cycle	E_{O1}/V	E_{R1}/V	ΔE_1/V	E_{O2}/V	E_{R2}/V	ΔE_2/V
1st	2.136	1.748	0.388	3.351	2.284	1.067
2nd	2.143	1.781	0.362	3.246	2.367	0.879
3rd	2.146	1.781	0.365	3.336	2.362	0.974
30th	2.246	1.712	0.534	3.347	2.292	1.055

found. Oxidation peak (E_{O2}) around 3.29V/Li can be ascribed to the oxidation of $LiFeBO_3$; Oxidation peak (E_{O1}) around 2.09V/Li can be associated with the oxidation of Fe(III) in $LiFeO_2$. This phenomenon is the same as the $LiFePO_4$–$Li_3V_2(PO_4)_3$ composite material, which reported by our group previously [20–22]. The two pairs of redox peaks during cycle, corresponding to the extraction/insertion of lithium ions from/into the bulk, which are in agreement with the charge/discharge curves (Fig. 5). The difference between oxidation and reduction peak potential (ΔV) is shown in Table 2. It becomes smaller during the first two cycles, and then becomes larger in the following cycles, the results are in accordance with the charge–discharge curves (Fig. 5).

4. Conclusions

A multi-layer core–shell $LiFeBO_3$/C cathode material has been synthesized successfully via spray-drying and carbothermal method. The XRD results show that a monoclinic $LiFeBO_3$ with some α-$LiFeO_2$ impurity are obtained. The Li/$LiFeBO_3$–C cell delivered an initial discharge capacity of 196.5 mAh g^{-1} and presented the stable discharge behavior ~136.1 mAh g^{-1} up to 30th cycle at the discharge current density of 10 mA g^{-1}. The surface sensitivity in the air was restrained, which attributes to the multi-layer core–shell structure. This multi-layer core–shell structure is quite meaningful for future industrial application of this cathode material.

Acknowledgment

This study was supported by National Natural Science Foundation of China (Grant No. 51302324 and 51272290).

References

[1] M. Armand, J.M. Tarascon, Nature 451 (2008) 652–657.
[2] D. Guyomard, J.M. Tarascon, J. Electrochem. Soc. 139 (1992) 937–948.
[3] A. Yamada, S.C. Chung, K. Hinokuma, J. Electrochem. Soc. 148 (2001) A224–A229.
[4] S.Y. Chung, J.T. Bloking, Y.M. Chiang, Nat. Mater. 1 (2002) 123–128.
[5] A.K. Padhi, K.S. Najundaswamy, J.B. Goodenough, J. Electrochem. Soc. 144 (1997) 1188–1194.
[6] V. Legagneur, Y. An, A. Mosbah, R. Portal, A.L. La Salle, A. Verbaere, D. Guyomard, Y. Piffard, Solid State Ionics 139 (2001) 37–46.
[7] X. Zhang, H. Guo, X. Li, Z. Wang, L. Wu, Electrochim. Acta 64 (2012) 65–70.
[8] A. Yamada, N. Iwane, Y. Harada, S. Nishimura, Y. Koyama, I. Tanaka, Adv. Mater. 22 (2010) 3583–3587.
[9] B. Zhang, J.C. Zheng, Electrochim. Acta 67 (2012) 55–61.
[10] F. Gao, Z. Tang, J. Xue, Electrochim. Acta 53 (2007) 1939–1944.
[11] F. Yu, J. Zhang, Y. Yang, G. Song, J. Solid State Chem. 14 (2010) 883.
[12] B. Huang, X. Fan, X. Zheng, M. Lu, J. Alloys Comp. 509 (2011) 4765–4768.
[13] P. Barpanda, Y. Yamashita, Y. Yamada, A. Yamada, J. Electrochem. Soc. 160 (2013) A3095–A3099.
[14] Y.Z. Dong, Y.M. Zhao, P. Fu, H. Zhou, X.M. Hou, J. Alloys Comp. 461 (2008) 585–590.
[15] K. Amine, H. Tukamoto, H. Yasuda, Y. Fujita, J. Eletrochem. Soc. 143 (1996) 1607–1613.
[16] Y.H. Rho, L.F. Nazar, L. Perry, D. Ryan, J. Electrochem. Soc. 154 (2007) A283–A289.
[17] J. Morales, J. Santos-Pena, R. Trocoli, et al., Electrochim. Acta 53 (2008) 6366–6371.
[18] Z.-j. Zhang, J.-z. Wang, S.-l. Chou, H.-k. Liu, O. Kiyoshi, H.-j. Li, Electrochim. Acta 108 (2013) 820–826.
[19] S.H. Bo, F. Wang, Y. Janssen, D.L. Zeng, K.W. Nam, W.Q. Xu, L.S. Du, J. Graetz, X.Q. Yang, Y.M. Zhu, J.B. Parise, C.P. Grey, P.G. Khalifah, J. Mater. Chem. 22 (2012) 8799–8809.
[20] J.-c. Zheng, X.-h. Li, Z.-xg. Wang, J. Power Sources 195 (2010) 2935–2938.
[21] J.-c. Zheng, B. Zhang, Z.-h. Yang, X. Ou, J.-f. Zhang, Bull. Chem. Soc. Jpn. 86 (2013) 376–381.
[22] J.-c. Zheng, X.-h. Li, Z.-x. Wang, J.-h. Li, L.-j. Li, L. Wu, Ionics 15 (2009) 753–759.